# Electric Pulses Induce Cylindrical Deformations on Giant Vesicles in Salt Solutions

Karin A. Riske and Rumiana Dimova
Max Planck Institute of Colloids and Interfaces, 14424 Potsdam, Germany

ABSTRACT In this article, we report for the first time unusual shape changes of vesicles subjected to strong electric pulses in salt solutions of low concentration. The electric field is created by two parallel electrodes between which the vesicle solution is located. Surprisingly, the vesicles assume cylindrical shapes during the pulse. These deformations are short-lived (their lifetime is ~1 ms) and occur only in the presence of salt outside the vesicles, irrespective of their content. When the solution conductivities inside and outside are the same, vesicles with square cross section are observed. Using a fast digital camera, we were able to record these deformations and study the vesicle shape dynamics. The aims of this article are to report the new vesicle morphologies and their dynamics and to provoke theoretical work in this direction.

## INTRODUCTION

The interaction of electric fields with lipid membranes and cells has been extensively studied in recent decades (1–4). The phenomena of electroporation and electrofusion, for example, are of particular interest because of their vast use in cell biology and biotechnology as means for cell hybridization or for introducing molecules such as proteins, foreign genes (plasmids), antibodies, or drugs into cells (5,6). Strong electric pulses of short duration induce transient pores across the cell membrane, thus allowing the influx/efflux of molecules and the possibility of fusion between two cells that are in close contact. Because electroporation occurs as a response of the lipid matrix to strong pulses, many studies on model lipid vesicles have been performed to gain knowledge on the process of electrical breakdown of lipid bilayers (7–9). In the last years, giant unilamellar vesicles (GUVs) were also used in such studies because they have the same dimensions as cells and allow direct observation using optical microscopy (4,10–17).

Apart from electroporating, lipid vesicles deform in response to electric fields (electrodeformation). When vesicles are subjected to electric fields, a potential builds across their membrane. As given by the Maxwell stress tensor, this transmembrane potential amounts to effective electrical tension (16,18). The vesicles are known to deform, assuming elliptical shapes. This effect has been studied theoretically both for alternating (AC) fields (19,20) and for square-wave direct current (DC) pulses (21,22). Experimental studies have shown that in AC fields of intermediate frequencies (~2 kHz), vesicles in pure water assume prolate deformation with the longer axis oriented along the field direction (23). At higher frequencies a prolate-to-oblate transition was reported (24,25) as theoretically predicted earlier (20,26). Varying the conductivities of the solutions inside and outside the vesicle also influences the vesicle shape. At fixed frequency (in the high frequency regime above several kilohertz), the vesicles assume oblate shapes when the external conductivity is higher and prolate shapes when the internal conductivity is higher (27). In a shape-analogous way, nonspherical cells have been observed to orient, rather than deform, parallel or perpendicular to the AC field, depending on the conductivity ratio and on the field frequency (1,28). Systematic studies on the behavior of giant vesicles at these conditions (various frequency and conductivity) are very scarce (27) even though GUVs would show the membrane behavior at cell-size scale.

The shape deformation induced on lipid vesicles by DC pulses was also predicted to depend on the ratio between the conductivities of the inner and outer vesicle solutions (21). This theoretical study predicts that, similarly to the effects in AC fields, a spherical vesicle would assume a prolate shape with the symmetry axis aligning parallel to the field for higher conductivity inside the vesicle and an oblate shape around the field for higher conductivity outside. Few experiments have been performed so far and mainly with nanosized salt-filled vesicles, for which the external conductivity is higher (29–31). These observations are indirect because of the small size of the vesicles, and cylindrical shapes such as those reported in this article cannot be resolved. Furthermore, in such systems, membrane tension and curvature are high and may play a significant role on the membrane behavior. The tension can essentially hinder morphological changes.

Microscopy studies on effects caused by electric pulses on giant vesicles are scarce. In the only study known to us, vesicles subjected to DC pulses and two different conductivity conditions have been observed to deform into prolates or oblates (10). However, the time resolution of these

*Submitted January 25, 2006, and accepted for publication June 1, 2006.*

Address reprint requests to R. Dimova, Max Planck Institute of Colloids and Interfaces, Science Park Golm, 14424 Potsdam, Germany. Tel.: 49-331-567-9615; Fax: 49-331-567-9612; E-mail: dimova@mpikg.mpg.de.

Karin A. Riske's present address is Instituto de Física da Universidade de São Paulo, São Paulo-SP, Brazil.



0006-3495/06/09/1778/09 $2.00

doi: 10.1529/biophysj.106.081620

observations (~1 image every 600 $\mu$s) is not sufficient to detect the cylindrical shape changes of the vesicles and their complete dynamic response as reported here. Video microscopy observations are difficult because the duration of the DC pulses is very short compared to standard video frequency (~20 frames per second (fps), i.e., one image every 50 ms). A possible solution to this problem is to slow down the vesicle response and relaxation by using a highly viscous solution, e.g., glycerin-water solution, as medium instead of water (12). Thus, it was possible to observe pore formation and closure at video frequency. However, this trick affects only the dynamic response, which depends on the bulk viscosity of the solution but, supposedly, not the membrane dynamics, which reflect the reorganization of the bilayer at shorter timescales. In addition, the presence of glycerin at high concentrations can lead to a change in the hydration of the lipids and, correspondingly, alter the membrane properties. An alternative method for stabilizing pores in giant vesicles is based on using conelike molecules favoring high curvature (32). However, this effectively implies changing the membrane composition because a relatively large fraction of these molecules (~10%) is required.

In our previous work (16), we used for the first time a fast imaging digital camera to record phase-contrast microscopy images of giant lipid vesicles subjected to DC pulses with a high temporal resolution, up to 30,000 fps (one image every 33 $\mu$s). In that article, we studied the deformation of GUVs in the absence of added salt (but still at higher conductivity of the internal solution), where the induced shape as a response to the external field was prolate, as theoretically predicted (21,22) and deduced from experiments on small vesicles (29–31).

In the work presented here, we use this fast imaging setup to present and discuss the different types of deformation imposed by DC pulses on spherical GUVs in salt solutions. Even though experimental conditions such as the presence of salt are much more physiologically relevant, they have not been explored thoroughly. In this study, we focus on the effects of salt on vesicle deformation induced by strong electric pulses. Intuitively, we expected to detect conductivity-dependent prolate or oblate shapes analogous to those observed in AC fields, and theoretically predicted for both AC fields and DC pulses. Surprisingly, when ions were present in the external medium, we found a new type of deformation, mainly cylindrical.

The article is organized as follows. After describing the materials and methods, we summarize the various types of deformations observed. Different conductivity ratios and external salt concentrations were explored. We discuss the vesicle shapes with respect to the membrane mechanical properties and tension (the relation to the tension induced by the electric field and the charging of the membrane is considered in detail in the Appendix). Afterward, we present data on the dynamics of vesicle deformations. Before concluding, we discuss a possible hypothesis for the appearance of the observed shapes. The theoretical approaches available in the literature (19,21,22) are not able to explain the cylindrical deformation of the vesicles. The results call for a novel theoretical model, which probably should account for ionic electrophoretic forces.

## MATERIALS AND METHODS

### Preparation of giant unilamellar vesicles

Giant unilamellar vesicles of L-$\alpha$-phosphatidylcholine from egg yolk, i.e., egg-PC (Sigma; St. Louis, MO), were grown using the electroformation method of Angelova and Dimitrov (33) and described in detail in Riske and Dimova (16). On several occasions, the vesicles were electroformed from the diblock copolymer polybutadiene-$\beta$-polyethyleneoxide ($PB_{32}PEO_{20}$) (34). The vesicles were swelled in 0.2 M sucrose and subsequently diluted 40 times into 0.2 M glucose solution, thus creating sugar asymmetry between the interior and the exterior of the vesicles. Furthermore, up to 1 mM NaCl was added to the sucrose solution (before electroformation) and up to 3 mM NaCl to the glucose solutions to set the desired conductivity asymmetry across the vesicle membrane. Note that performing vesicle electroformation in the presence of salt at higher concentration was not successful. However, salt concentrations as low as 1 mM were not observed to affect the electroformation process. The osmolarities of the inner and the outer solutions were measured with a cryoscopic osmometer Osmomat 030 (Gonotec, Berlin, Germany) and carefully matched with glucose to avoid osmotic pressure effects. The conductivities of the internal and the external solutions were measured with a conductivity meter SevenEasy (Mettler Toledo, Greifensee, Switzerland). The conductivities of the salt-free sucrose and glucose solutions were measured to be between 6 $\pm$ 1 and 4.5 $\pm$ 1 $\mu$S/cm, respectively (yielding conductivity ratio of inner versus outer solution conductivity of ~1.3). The maximum conductivity of the electroformation solutions containing salt was 120 $\mu$S/cm. Unless mentioned otherwise, the subsequent data were acquired for vesicle solutions where the conductivity has been adjusted with NaCl. In some cases, instead of NaCl we used buffers containing 0.1 mM $Ca^{2+}$ and $Mg^{2+}$ acetates, BSA, and sorbitol, but no difference in the vesicle behavior was observed. Even though it was interesting to compare the effect of monovalent ions (i.e., $Na^{+}$) with divalent ones ($Ca^{2+}$), higher $Ca^{2+}$ concentrations were avoided because calcium is known to adsorb on membranes, alter the bilayer properties, and effectively induce membrane tension (35).

Finally, the diluted vesicle solution was placed in an observation chamber where the DC pulses were applied. Because of the density difference between the sucrose and glucose solutions, the vesicles settled at the bottom of the chamber where they were easy to locate. The refractive index difference produced a good optical contrast of the images when phase contrast microscopy was used (the vesicles appear as dark objects on a light gray background). In addition, the sugar asymmetry made it possible to observe vesicle electroporation. The pores are detected due to efflux of the dark sucrose solution out of the vesicle. This efflux usually disrupts the bright halo observed around the vesicles (see the example available in the online Supplementary Material). The osmotic stabilization of the vesicles assured volume conservation throughout the measurements except possibly for the cases when poration of the membrane was induced, but even then, no change in the vesicle volume was detected.

### Optical microscopy

An inverted microscope, Axiovert 135 (Zeiss, Göttingen, Germany) equipped with a 20× Ph2 objective, was used to visualize the GUVs. A fast digital camera, HG-100 K (Redlake, San Diego, CA), was mounted on the microscope and connected to a PC. Image sequences were acquired at 20,000 fps and 30,000 fps, with picture resolution of 2.75 pixels/$\mu$m and

1.68 pixels/$\mu$m, respectively. For routine observations and the vesicle selection, the sample was illuminated with a halogen lamp. A mercury lamp HBO W/2 was used only for a short time of up to ~10 s during the recording of the snapshot sequences with the fast digital camera. Sample heating from the illumination was measured using a thermocouple probe (Keithley Instruments, Cleveland, OH) immersed in the sample before and after an experimental observation of ~10 min. The change in temperature was <2°C and thus did not significantly change the bilayer properties.

The observation chamber, purchased from Eppendorf (Hamburg, Germany), consists of a Teflon frame confined above and below by two glass plates through which observation was possible. A pair of parallel electrode wires (92 $\mu$m in radius) were fixed to the lower glass at a gap axial distance of 475 ± 5 $\mu$m. This small interelectrode distance practically assures a homogeneous field in the space between the electrodes (for effects of electrode geometry on field homogeneity, see Miklavčič et al. (36)). The chamber was connected to a Multiporator (Eppendorf), which generated square-wave DC pulses. The pulse strength and duration could be set in the range 5–300 V (0.1 ± 0.01 to 6 ± 0.6 kV/cm) and 5–300 $\mu$s, respectively. Time 0 in the recorded sequences was defined as one frame before visible vesicle deformation occurred. Because occasional drifts of the vesicles with time were observed, we assume that there was no membrane adhesion to the glass surface.

## RESULTS

### Types of deformations

The deformation shapes of giant unilamellar vesicles subjected to DC pulses were investigated for different conductivity conditions for the inner and outer vesicle solutions. The salt concentrations inside and outside the vesicles, $c_{in}$ and $c_{out}$, respectively, were varied between 0 and 3 mM, thus covering a large interval of conductivity ratios $x = \lambda_{in}/\lambda_{out}$, where $\lambda_{in}$ and $\lambda_{out}$ are the conductivities of the inner and outer vesicle solutions, correspondingly (note that salt-free solutions have finite conductivity). Fig. 1 shows some snapshot examples of vesicles at different conductivity ratios and data for more than 30 vesicles, where mainly NaCl was used to tune the solution conductivities. Using buffers containing $Ca^{2+}$ and $Mg^{2+}$ acetates produced no difference in the observed behavior. Due to concerns related to changes in the vesicle content caused by electroporation, which can possibly lead to a change in the internal conductivity, the vesicles used for measuring conductivity effects on the degree of deformation have been subjected to a pulse for the first time. Thus, the indicated conductivity ratios are accurate. Even in cases when the vesicles were subjected to several consecutive pulses, no change in the volume was observed, and the gray-value intensity of the vesicle images was preserved, indicating that there was no detectable amount of glucose–sucrose solution exchange between the vesicle interior and the external solution. In the absence of salt in the vesicle exterior (irrespective of the internal salt concentration $c_{in}$), the induced vesicle shape is prolate (Fig. 1 *B*). The presence of salt in the outer solution causes flattening of the vesicle sidewise; i.e., the vesicles assume cylindrical shapes with spherical caps. The observed deformations have either a disklike geometry ($a/b < 1$) for $x < 1$ (Fig. 1 *C*) or a tubelike shape ($a/b > 1$) for $x > 1$ (Fig. 1 *E*). The intermediate case

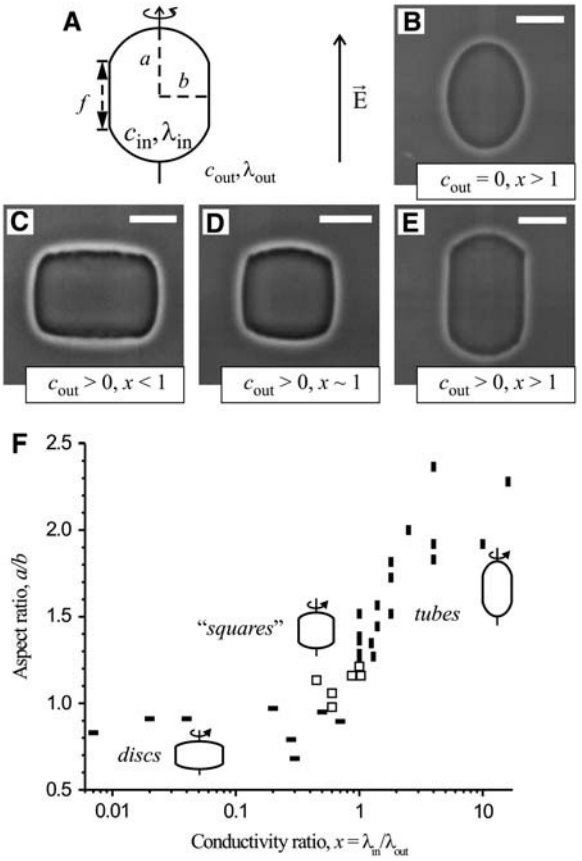


FIGURE 1 Deformation of vesicles at different conductivity conditions subjected to DC pulses. (*A*) Schematic illustration of a cross section of a vesicle, which has assumed a cylindrical deformation when salt is present in the vesicle exterior. The field direction is indicated with an arrow. (*B*) In the absence of salt in the external solution, prolate deformation is observed. The presence of salt flattens the vesicle walls: disklike (*C*), ''square''-like (*D*), and tubelike (*E*) vesicles. The scale bars correspond to 15 $\mu$m. (*F*) Data on the maximum aspect ratio $a/b$ reached for vesicles at different conductivity conditions when subjected to DC pulses of strength $E = 2$ kV/cm and duration $t_p = 200$ $\mu$s.

($x \sim 1$) has a cross section similar to a square ($a/b \sim 1$) (Fig. 1 *D*). Here $a$ and $b$ are the vesicle semiaxis along and perpendicular to the applied field (see sketch in Fig. 1 *A*). To confirm this general trend in the vesicle deformation behavior, i.e., the dependence of the aspect ratio $a/b$ on the conductivity ratio $x$, we performed measurements on many vesicles of which only vesicles subjected to a DC pulse for the first time were included in Fig. 1 *F*. Even though some scatter in the data is observed, which will be discussed further, a clear trend of the dependence $a/b$on $x$ as discussed above is observed.

It is interesting to compare the morphologies induced by DC pulses with the deformations of vesicles subjected to AC fields (27) at similar conductivity conditions. At intermediate field frequencies (e.g., about several tens of kilohertz) vesicles at $x < 1$ assume oblate shapes ($a/b < 1$), analogous to the disklike deformation, whereas for $x > 1$ the vesicles

deform into prolates ($a/b > 1$), analogous to the tubelike shapes. However, in AC fields, no flattening of the vesicles is observed.

We can summarize that the conductivity ratio, $x$, sets the direction of the vesicle elongation in respect to the electric field (parallel when $x > 1$ and perpendicular when $x < 1$). Yet, a comparison between Fig. 1, *B* and *E* demonstrates that the presence of salt in the external medium adds a perpendicular compressive force, which flattens the vesicle walls during the DC pulse. Performing experiments with lipid vesicles and with polymersomes (vesicles made of diblock copolymers) showed no difference in the morphological response. Thus, we conclude that the effect is mainly due to the presence of salt and not due to the membrane characteristics. Cylindrical deformations have not been observed on cells (37,38). However, the temporal resolution in those experiments (3.3 ms per image) is not high enough to detect short-lived deformations (of lifetime approximately a few hundred microseconds) as reported here. The vesicle elongation as a function of the conductivity ratio $x$ has already been theoretically predicted in the literature (21,22), but the short-lived vesicle compression perpendicular to the field (i.e., flattening, or cylindrical deformation) has not been predicted or reported so far.

The type of deformation, i.e., whether a vesicle deforms into a disk, a ''square'', or a tube, depends on the conductivity ratio $x$. The degree of deformation for a fixed $x$ depends mainly on the membrane tension and the excess area of the vesicle. Flaccid, tension-free vesicles are easy to deform, as the energy scale is set by the bending modulus of the membrane $\kappa$. Both for egg-PC vesicles and for polymersomes $\kappa \sim 10^{-12}$ erg (27,34,39). The energy needed to deform a fluctuating vesicle is $\sim 2\pi\kappa \sim 10^{-11}$ erg. On the other hand, the larger the excess area is (as compared to the area of a spherical vesicle of the same volume), the larger the deformation is. Thus, the observed scatter in $a/b$ in Fig. 1 *F* results from vesicles with different excess area and tension. The vesicles studied in this work were spherical (tense) or quasispherical (tension-free and with visible thermal fluctuations). Tense vesicles are more difficult to deform because the shape transformation requires work $\sim(1/2)K(\Delta A)^2/A_0$ to stretch the membrane, where $K$ is the stretching elasticity modulus, $\Delta A$ is the area change, and $A_0$ is the initial vesicle area. For egg-PC, $K \sim 140$ dyn/cm (40); thus, for a vesicle with a radius 20 $\mu$m, the energy needed to increase the area by 1% is $\sim 4 \times 10^{-7}$ erg. Electric fields can transfer such energies to the membrane, inducing a perpendicular stress in the bilayer (compression). Because the bilayer is almost incompressible, this stress results in an increase in the membrane area. Thus, the electric field causes an extra tension to the vesicle, also referred to as an electric tension (16,18,41); see the Appendix for definition. The latter depends on the pulse strength and duration. Once the field is on, the bilayer begins to charge, and the electric tension gradually builds up, defining the maximal deformation of the vesicle. For longer or stronger pulses, the bilayer porates; see next section and Appendix for poration conditions. Fig. 2 shows snapshots of the maximal deformations of a vesicle that was subjected to a sequence of pulses of different field strength $E$ and duration $t_p$. The snapshots were taken typically at the end of the applied pulse. The stronger the field (Fig. 2 *A*) or the longer the pulse (Fig. 2 *B*) is, the more the vesicle deforms.

## Vesicle poration

When the transmembrane potential induced by the pulse reaches a critical value $V_c \sim 1$ V, electroporation occurs. As discussed in detail in the Appendix, the transmembrane potential is maximal at the vesicle poles and depends on the electric field strength $E$, the vesicle radius $R$, and the membrane charging time $\tau_{charg}$. The last is shorter, the higher the inner and outer conductivities are. Typical values of $\tau_{charg}$ estimated for the conductivity conditions in this work lie between 10 and 560 $\mu$s. However, $V_c$ can be reached at a critical time $t_c < \tau_{charg}$. For example, for the vesicle in Fig. 2, the poration condition $V_c = 1$ V is reached at $t_c = 143, 60, 40,$ and 30 $\mu$s for $E = 1, 2, 3,$ and 4 kV/cm, respectively, whereas the charging time is $\tau_{charg} = 300$ $\mu$s. In most of the cases discussed here, the pulse strength and duration used were enough to induce electroporation ($t_c < t_p$). Detecting pores on vesicles is not always possible. Macropores of sizes above a couple of micrometers in diameter are usually visualized by leakage of sucrose from the vesicle interior to the external solution (16). Because of the refractive index difference of the two solutions, one can observe the efflux when the pores are located in the vesicle focal plane of observation. Examples

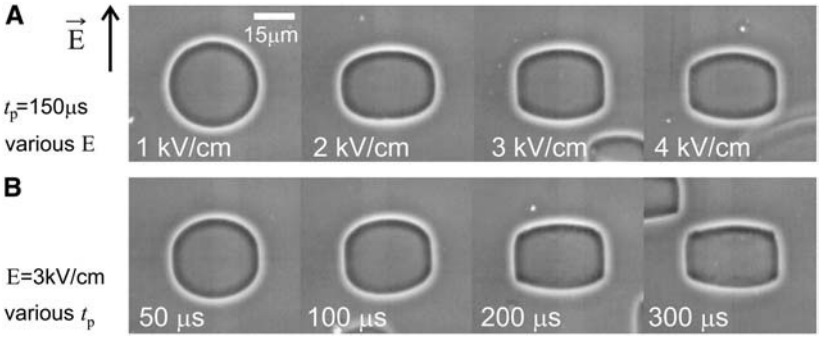


FIGURE 2 Effect of pulse strength and duration on the deformation of a vesicle of radius $R = 17.6$ $\mu$m. The conductivity conditions are $x = 0.05$, $\lambda_{in} = 6$ $\mu$S/cm, $\lambda_{out} = 120$ $\mu$S/cm, $c_{in} = 0$, $c_{out} = 1$ mM NaCl. The field direction is shown with an arrow in the upper left corner. (*A*) Maximum deformation observed for various $E$ and $t_p = 150$ $\mu$s (the field strength is indicated on each snapshot). (*B*) Maximum deformation observed for various $t_p$ and $E = 3$ kV/cm (the pulse duration $t_p$ is indicated on each snapshot).

from porated vesicles at two different conductivity conditions, $x > 1$ and $x < 1$, are given in Fig. 3, where the pores are indicated with arrows. The vesicle deformation dynamics are discussed in the next section. Another example for vesicle poration is given in the online Supplementary Material. Often the vesicles are observed to porate at the rims of the spherical caps. Even when the condition for poration is reached, pores may not be detected because they can be out of the focal plane of observation, or their size might be below the microscope resolution. Irrespective of the poration conditions, cylindrical deformations were always detected as long as salt was present in the vesicle exterior.

## Deformation dynamics

The vesicle shape dynamics as a response to DC pulses for vesicles in salt-free solutions have been studied and discussed in detail in our previous work, where the induced deformation was always prolate (16). In that case the vesicle geometry could easily be quantified in terms of the ratio $a/b$. With salt present in the external solution, cylindrical vesicles with rounded caps are the shapes induced by DC pulses. The ratio $a/b$ is not enough to define this type of vesicle deformation because the length of the flat equatorial band with width $f$ is an additional geometric characteristic (see Fig. 1 *A*). Thus, the two dimensionless parameters defining the whole deformation shape are $a/b$ and $f/d$, where $d$ is the diameter of the spherical vesicle before the pulse. The change in $a/b$ will be referred to as ''elongation'', and the change in $f/d$ as ''flattening''. The two are interrelated because the increase in $f$ acts against the increase in $b$.

The dynamics of vesicle elongation as a function of $x$ have already been theoretically treated (22) and, for the prolate case (absence of salt in the outer solution), found to be in qualitative agreement with the data (16). But the flattening of the vesicle (cylindrical deformation) in the presence of salt, to our knowledge, is a novel observation. Fig. 3 shows the deformation dynamics of vesicles in salt solutions, both for $x > 1$ (Fig. 3 *A*) and for $x < 1$ (Fig. 3 *B*). The behavior of one of those vesicles (larger vesicle in Fig. 3 *B*) subjected to a sequence of pulses was investigated in detail to assess the deformation quantitatively. The maximum deformations of this same vesicle at different pulses were given in Fig. 2. The flattening ($f/d$) and elongation ($a/b$) dynamics of the vesicle are shown in Fig. 4 for $E = 3$ kV/cm and various pulse duration $t_p$. The poration time $t_c = 40$ $\mu$s does not seem to have any influence on the flattening dynamics; within the experimental accuracy for measuring $f/d$, we do not observe any significant hump in the data due to the vesicle poration for this and for other vesicles with different poration times. The error in $f$ is large ($\leq$20%) because for small deformations, the rounded edges of the vesicles make the measurement difficult.

Another notable feature in the vesicle response dynamics is seen in the first few hundreds of microseconds after application of the pulse (Fig. 4). The flattening response ($f/d$) occurs faster than the elongation ($a/b$). As an example, we have emphasized the pulse of duration $t_p = 300$ $\mu$s shown with star symbols (the time sequence shown in Fig. 3 *B*, lower right vesicle, corresponds to this data set). The arrows indicate the time when a maximum in the $f/d$ and $a/b$ deformation is reached. The response in $f/d$ is completed at $\sim$100 $\mu$s, which is when the $a/b$ elongation takes over and reaches a maximum value approximately at the end of the pulse ($\sim$300 $\mu$s). The difference in the response times of flattening and elongation suggests that the two types of deformations have different origins. The relaxation times obtained from exponential fits to the data are also different: for the pulse of duration 300 $\mu$s, these times were $\tau_{a/b} = 5.3 \pm 0.4$ ms and $\tau_{f/d} = 1 \pm 0.6$ ms. On average, from all measurements performed on many vesicles, we find $\tau_{a/b} = 4.6 \pm 3$ ms and $\tau_{f/d} = 1.5 \pm 1$ ms. No trend in $\tau_{a/b}$ and $\tau_{f/d}$ was observed with pulse number or strength/duration. As mentioned above, almost all pulses induced transmembrane potentials above the electroporation limit. Thus, it is reasonable that $\tau_{a/b}$ is very close to the characteristic relaxation time measured for porated vesicles in the absence of salt, $\sim 7 \pm 4$ ms (16). In that work, $\tau_{a/b}$ was found to be related to the resealing of the membrane. The driving force for the process of pore closure is the edge tension of the pore that originates from the energetic cost to rearrange or curve the

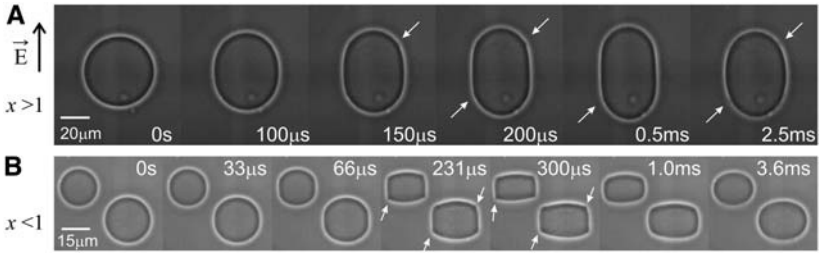


FIGURE 3 Time sequences from the deformation dynamics of vesicles in two different conductivity conditions. The field direction is indicated in the upper left corner. Arrows indicate the formation of small pores visualized by the efflux of dark sucrose solution out of the vesicles. The time of snapshot acquisition is indicated in the lower or upper right corner of each image. (*A*) Tubelike deformation of a vesicle of $R = 24.1$ $\mu$m at conductivity conditions $x = 1.38$, $\lambda_{in} = 16.5$ $\mu$S/cm, $\lambda_{out} = 12$ $\mu$S/cm, $c_{in} = 0.1$ mM NaCl, and $c_{out} = 0.05$ mM NaCl. The pulse parameters are $E = 2$ kV/cm and $t_p = 200$ $\mu$s. The charging time is $\tau_{charg} = 246$ $\mu$s, and the poration time is $t_c = 37$ $\mu$s. The acquisition frequency was 20,000 fps. (*B*) Disklike deformation of two vesicles of radius 10.0 $\mu$m (*left*) and 17.6 $\mu$m (*right*, same vesicle as in Fig. 2). The conductivity conditions are given in the caption of Fig. 2. The pulse parameters are $E = 3$ kV/cm and $t_p = 300$ $\mu$s. The charging time for the larger vesicle is $\tau_{charg} = 300$ $\mu$s, and for the smaller one $\tau_{charg} = 171$ $\mu$s. The poration times are $t_c = 40$ and 43 $\mu$s, respectively. The acquisition frequency was 30,000 fps. Another example for vesicle poration and movies of the full time course of the deformation of vesicles at different $x$-conditions are available in the online Supplementary Material.

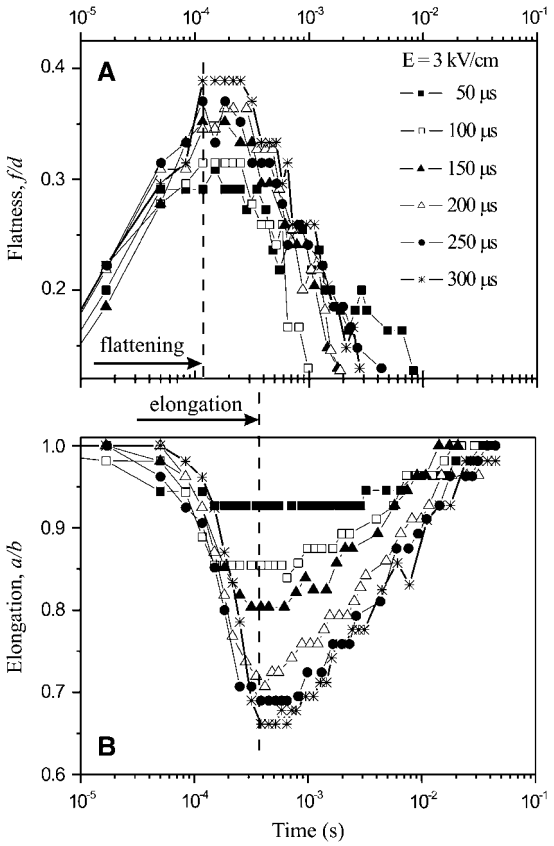


FIGURE 4 Deformation dynamics of the flattening $f/d$ (*A*) and the elongation $a/b$ (*B*) of a vesicle of radius 17.6 $\mu$m (shown in Figs. 2 and 3 *B*, vesicle on the *right*) subjected to a sequence of pulses with strength $E = 3$ kV/cm and increasing duration $t_p$ (see legend). The camera acquisition frequency was 30,000 fps. The conductivity conditions are given in the caption of Fig. 2. The charging and poration times are $\tau_{charg} = 300$ $\mu$s and $t_c = 40$ $\mu$s. The time ranges for achieving the maximum in the vesicle flattening ($f/d$) and in the elongation response ($a/b$) are indicated with dashed lines for the pulse duration of $t_p = 300$ $\mu$s (*star symbols*).

lipid molecules on the edge of the pore. The edge energy per unit length $\gamma$ can be estimated to be $\kappa/2h$, where $h$ is the membrane thickness (~4 nm). Thus, $\gamma$ is on the order of $10^{-6}$ dyn (42). The characteristic time for pore closure is given by $\eta_s r_{pore}/(2\gamma)$ (16), where $r_{pore}$ is the pore radius and $\eta_s$ is the membrane shear viscosity, yielding several milliseconds, which is in agreement with the values obtained for $\tau_{a/b}$. It is normal that $\tau_{f/d}$ differs. The membrane in the equatorial region of the vesicle does not charge (see Eq. 1 in the Appendix). Thus, poration in the flat area does not occur, and therefore, the relaxation behavior is not related to the characteristic times of pore closure.

## Possible explanations for the cylindrical shape deformation

Various ideas can be considered as to the possible cause for this curious phenomenon of cylindrical deformation. In this section, we discuss some of them.

### *Lipid-specific effects*

Experiments performed on polymersomes showed the same cylindrical deformation in the presence of salt as observed for lipid vesicles. Therefore, lipid-specific effects, e.g., partial headgroup charge and membrane thickness, as a possible cause for the observed cylindrical deformations are to be excluded. It will be interesting to perform a detailed study on the behavior of partially charged vesicles, for example, composed of lipid mixtures of phosphatidylcholine and phosphatidylglycerol or phosphatidylcholine and phosphatidylserine. Presumably, the redistribution of charges in the membrane may lead to interesting morphological responses of the vesicles.

### *Effect of electropermeabilization and local change in membrane properties*

As an alternative explanation for the observed cylindrical deformations, one can consider the possibility of local changes in the properties of the membrane when subjected to pulses. The impact of the electric field on the initially spherical vesicles is concentrated on the vesicle poles (see Eq. 1 in the Appendix); thus, inhomogeneity in the state of the membrane along the vesicle surface is to be expected. In particular, shortly after the field is applied, the membrane tension can vary in different parts of the vesicle, e.g., at the poles reaching values close to the lysis tension while at the equator remaining unchanged. We do not exclude that the cylindrical deformations can be influenced by such inhomogeneity in the membrane tension. Nevertheless, if the flattening deformation was only due to tension inhomogeniety, such an effect should be expected also for vesicles in absence of salt for pulses leading to similar transmembrane potentials or charging times. However, comparing vesicles at such conditions clearly shows that only vesicles in the presence of salt in the external medium assume cylindrical deformation.

In this work, for almost all of the observed vesicles, the transmembrane potential exceeded the poration threshold of 1 V/cm. However, one cannot claim that the detected cylindrical deformations are specific to electropermeabilized membranes because for porated vesicles in salt-free solutions flattening is not observed (16). Thus, a hypothesis based only on change in the mechanical properties of membranes in the electropermeabilized state cannot explain the shapes reported in this work.

### *Ion electrophoretic forces*

The hypothesis we favor most is related to electrophoretic forces exerted by the ions. When the field is applied, the cations and anions exhibit directed motion toward the respective electrode of opposite charge (indicated with *arrows* in Fig. 5). The ions whose motion, due to the field, is blocked by the vesicle (see the ''shielded volume'' in Fig. 5) hit the membrane. We consider only the ions located in a cylindrical

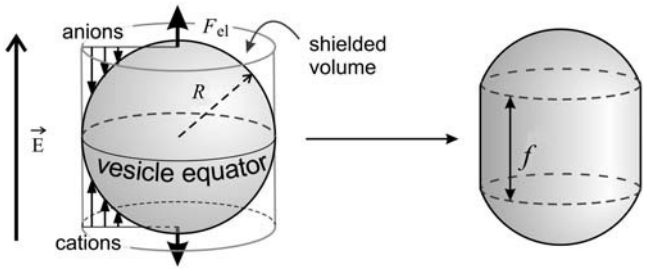


FIGURE 5 Illustration on the hypothesis of vesicle wall flattening induced by ions in the external solution. The cylindrical volume around the vesicle (''shielded volume'') indicates the zone with the ions that take part in the ''flattening''. The rest of the ions in the solution outside this volume are not taken into account, as they would mainly influence the vesicle absolute position, which in the experiments is not observed to change. The arrows indicate the directions of the anions and cations moving when the field is on. The field direction is also shown.

space around the vesicle because the effect of the rest of the ions above and below this volume would result in an overall displacement of the vesicle center of mass, which is not observed. Once the field is on, the impact from the ion displacement should be more pronounced at the vesicle equatorial zone as the shielded volume above and below this area is larger; i.e., there the number of ions reaching and hitting the membrane is larger. Thus, the ions effectively iron the vesicle in the equatorial zone. At the same time, the field causes an overall elongation or compression of the vesicle (as symbolically indicated with the force $F_{el}$ in Fig. 5) depending on $x$ as predicted (22).

The applied field quickly accelerates the ions, and they reach a steady velocity $v = uE$, where $u$ is the ion mobility. For chloride ions, $u \sim 8 \times 10^{-8}$ $m^2s^{-1}V^{-1}$ and for typical values of the field strength, $E = 3$ kV/cm, one obtains $v \sim 2.4$ cm/s. The kinetic energy of the ion is $mv^2/2$ where $m$ is the ion mass ($m \sim 6 \times 10^{-23}$ g for $Cl^-$). We sum this energy over all the ions present in the volume shielded by the vesicle, $\sim 2R^3$ (Fig. 5), where $R \sim 20$ $\mu$m is the vesicle radius. At a typical concentration of 1 mM of salt, the total energy one obtains is $\sim 10^{-12}$ erg, which is enough to bend the membrane (see above). This simple estimate shows that a scenario that assumes that the ions play the main role in the observed membrane flattening is energetically possible.

The electric tension in the area of the flat band is negligible, in particular in the early time after the pulse application (see Eq. 3 in the Appendix), which is why we compared the energy applied by the ions with bending deformations. At a later stage, when the tension at the vesicle poles has reached higher values, the energy contributed by the ions is no longer enough to dominate the vesicle deformation. Then, the flattening is suppressed (see Fig. 4), and the overall vesicle deformation is dominated by stretching, which is expressed in the dynamics of $a/b$.

Being concerned about a change in the conductivity inside and outside the vesicle during the pulse, we estimated the approximate travel distance of ions during the pulse. For a DC pulse of duration $t_p = 100$ $\mu$s and velocity of 2.4 cm/s (as calculated above for $E = 3$ kV/cm), the maximum travel distance of an ion would be $\sim 2.5$ $\mu$m, and less than a micrometer for weaker fields. Compared to typical vesicle sizes ($\sim 20$ $\mu$m), and taking into consideration the very low ionic concentration, we conclude that only a small number of ions would make their way through the electroporated membrane. Furthermore, due to the sign of the Laplace pressure, only loss of internal volume occurs when a pore opens. Therefore, the internal conductivity is conserved, and the leaking volume is so small that it effectively does not change the conductivity of the external medium. Thus, the change in the conductivity conditions would be negligible. This was not the case for erythrocyte membranes in more concentrated salt solutions ($\sim 150$ mM NaCl) and much higher conductivity (43). However, in our system, typical conductivities are $\sim 100$ times lower.

The hypothesis about membrane flattening due to electrophoretic ionic forces can be tested if one performs measurements on vesicles with same $x$, excess area and vesicle tension, but different $c_{out}$. Such conditions are difficult to achieve because vesicle size and tension are not controllable parameters during preparation. In addition, to compare deformations with similar aspect ratios $a/b$, one has to keep the conductivity ratio $x$ the same, and thus, with increasing $c_{out}$, one needs vesicles with larger $c_{in}$. However, preparing vesicles at higher salt concentration is not an easy task. Presumably, it might be possible to test this hypothesis using various ions. However, the choice for salts should be such that interaction of the ions with the membrane should be avoided. We have already examined ions such as calcium, magnesium, and acetate, but even though they have higher mass, their mobility is lower; thus, they do not produce a measurable effect. Another idea on examining the electrophoretic effect of ions would be to test oil droplets in salt solutions subjected to DC pulses; however, producing a stable emulsion involves the use of surfactants, which may introduce complexity to the system.

## CONCLUDING REMARKS

In the absence of salt in the vesicle exterior, giant vesicles assume elliptical shapes as a response to DC pulses, as discussed previously (16). But in the presence of salt, unusual cylindrical shape transformations were observed. Of course, nonstandard vesicle shapes can be induced by inhomogeneous electric fields (e.g., in octode field cages (44)) or by magnetic fields acting on vesicles filled with magnetic nanoparticles (45). In this work, however, we demonstrate that even the simplest field configuration of two parallel electrodes induces nontrivial vesicle shapes. We have studied the response of giant vesicles to DC pulses in different conductivity conditions. We found that the conductivity ratio is not the only parameter defining the vesicle deformation as a response to

DC pulses, as theoretically predicted (21,22). The presence of salt in the external vesicle medium, irrespective of the conductivity ratio $x$, adds a compressive force perpendicular to the field, which forces the vesicle walls to align parallel to the field. In this way, cylindrical vesicles with rounded caps are the observed shapes as a response to DC pulses. The conductivity ratio $x$ defines whether the vesicle elongates and deforms into a tube ($\lambda_{in} > \lambda_{out}$, or $x > 1$) or into a disk ($\lambda_{in} < \lambda_{out}$, or $x < 1$). These deformations are not equilibrium shapes and have a very short life time, on the order of 1 ms, which is why they are not detected at standard video acquisition speed. Presumably, similar shapes are to be observed in cells at physiological conditions because of the presence of salt in the extracellular solution. Using a fast digital camera we were able to record these deformations on giant vesicles for the first time and study the dynamics of vesicle response and relaxation. We hope that this report provokes theoretical work to explain the observed phenomenon.

## APPENDIX: ELECTRIC TENSION AND ELECTROPORATION

When vesicles are subjected to an electric field, charges accumulate at the bilayer interface, creating a transmembrane potential, $V_m$, across the nonconductive membrane (46):

$$V_m = 1.5\,R\cos\theta E(1 - e^{-t/\tau_{charg}}), \quad (1)$$

where $R$ is the vesicle radius, $E$ is the applied electric field, $\theta$ is the angle between the electric field and the vesicle surface normal, $t$ is time, and $\tau_{charg}$ is the membrane charging time. For the vesicle membrane located in the equatorial zone or in the flat areas parallel to the field direction (where $\theta = 90°$), the bilayer remains uncharged, implying that the transmembrane potential is zero in the equatorial band of cylindrical vesicles.

The membrane charging time is given by (46)

$$\tau_{charg} = RC_m[1/\lambda_{in} + 1/(2\lambda_{out})]. \quad (2)$$

Here $C_m$ is the membrane capacitance, $\sim 1\ \mu F/cm^2$ for lipid membranes (18,47). The charging time decreases with the increase in both internal and external conductivities, $\lambda_{in}$ and $\lambda_{out}$. For the limited case of salt-free solutions, discussed in our previous work (16), and for a typical vesicle radius $R = 15\ \mu m$, $\tau_{charg} \sim 415\ \mu s$. For the various conductivity conditions $\lambda_{in}$ and $\lambda_{out}$, and for the different vesicle radii $R$ discussed in this work, the charging times range between 10 and 560 $\mu s$. For the intermediate case of no salt inside and 1 mM NaCl outside, $\tau_{charg} \sim 300\ \mu s$.

The transmembrane potential $V_m$ causes an increase in the membrane lateral tension. This contribution, also called electric tension $\sigma_{el}$, is expressed in terms of $V_m$ as (18,41):

$$\sigma_{el} = \varepsilon\varepsilon_o(h/2h_e^2)V_m^2 \quad (3)$$

where $\varepsilon$ is the dielectric constant of the aqueous solution, $\varepsilon_o$ the vacuum permittivity, $h \sim 39$ Å is the total bilayer thickness, and $h_e \sim 28$ Å the dielectric thickness, both measured for lecithin bilayers (48). Electroporation occurs when the lateral tension exceeds the membrane lysis tension $\sigma_{lys}$ (for lipid membranes $\sigma_{lys}$ is typically 6 dyn/cm) (16,18). For an initially tension-free vesicle, this corresponds to a critical transmembrane potential $V_c \sim 1$ V. If the vesicle has some initial tension, then $V_c$ will be lower, as poration will occur whenever the total vesicle tension, which is the sum of the initial tension and the electric tension, reaches $\sigma_{lys}$.

The charging times discussed above can be longer or shorter than the pulse duration, $t_p$. However, even if $t_p < \tau_{charg}$, electroporation will occur at a critical time $t_c$, when $V_c$ is reached on the vesicle poles facing the electrodes ($\theta = 0°$, see Eq. 1). Throughout the work, we estimate $t_c$ assuming $V_c = 1$ V (which is the value for tension-free vesicles) because we are not able to measure the initial tension of the vesicles studied here. The critical times $t_c$ are given in the text or in the figure captions for the specific vesicles investigated.

## SUPPLEMENTARY MATERIAL

An online supplement containing time sequences with snapshots of a porated vesicle and movies can be found by visiting BJ Online at http://www.biophysj.org.

We are grateful to R. Lipowsky for support and enlightening discussions. J. Shillcock is acknowledged for stimulating interactions, and M. Prevot for proofreading the text. We thank S. Aranda and D. Dudas for their help and cheerful attitude.

## REFERENCES

1. Zimmermann, U. 1982. Electric field-mediated fusion and related electrical phenomena. *Biochim. Biophys. Acta*. 694:227–277.
2. Neumann, E., A. E. Sowers, and C. A. Jordan. 1989. Electroporation and Electrofusion in Cell Biology. Plenum Press, New York.
3. Chang, D. C., B. M. Chassey, J. A. Saunders, and A. E. Sowers, editors. 1992. Guide to Electroporation and Electrofusion. Academic Press, New York.
4. Lipowsky, R., and E. Sackmann. 1995. Structure and Dynamics of Membranes. Elsevier Science B. V., Amsterdam.
5. Zimmermann, U. 1986. Electrical breakdown, electropermeabilization and electrofusion. *Rev. Physiol. Biochem. Pharmacol*. 105:175–256.
6. Tekle, E., R. D. Astumian, and P. B. Chock. 1994. Selective and asymmetric molecular transport across electroporated cell membranes. *Proc. Natl. Acad. Sci. USA*. 91:11512–11516.
7. Teissie, J., and T. Y. Tsong. 1981. Electric field induced transient pores in phospholipid bilayer vesicles. *Biochemistry*. 20:1548–1554.
8. Glaser, R. W., S. L. Leikin, L. V. Chernomordik, V. F. Pastushenko, and A. I. Sokirko. 1988. Reversible electrical breakdown of lipid bilayers: formation and evolution of pores. *Biochim. Biophys. Acta*. 940:275–287.
9. Kakorin, S., T. Liese, and E. Neumann. 2003. Membrane curvature and high-field electroporation of lipid bilayer vesicles. *J. Phys. Chem. B*. 107:10243–10251.
10. Kinosita. K., M. Hibino, H. Itoh, M. Shigemori, K. Hirano, Y. Kirino, and T. Hayakawa. 1992. Events of membrane electroporation visualized on a time scale from microseconds to seconds. *In* Guide to Electroporation and Electrofusion. D. C. Chang, B. M. Chassey, J. A. Saunders, and A. E. Sowers, editors. Academic Press, New York. 29–46.
11. Zhelev, D. V., and D. Needham. 1993. Tension-stabilized pores in giant vesicles: determination of pore size and pore line tension. *Biochim. Biophys. Acta*. 1147:89–104.
12. Sandre, O., L. Moreaux, and F. Brochard-Wyat. 1999. Dynamics of transient pores in stretched vesicles. *Proc. Natl. Acad. Sci. USA*. 96: 10591–10596.
13. Tekle, E., R. D. Astumian, W. A. Friauf, and P. B. Chock. 2001. Asymmetric pore distribution and loss of membrane lipid in electroporated DOPC vesicles. *Biophys. J*. 81:960–968.
14. Aranda-Espinoza, H., H. Bermudez, F. S. Bates, and D. E. Discher. 2001. Electromechanical limits of polymersomes. *Phys. Rev. Lett*. 20: 208301.
15. Lee, C.-H., Y.-F. Chang, C.-H. Tsai, and P.-H. Wang. 2005. Optical measurement of the deformation of giant lipid vesicles driven by a micropipet electrode. *Langmuir*. 21:7186–7190.

16. Riske, K., and R. Dimova. 2005. Electro-deformation and -poration of giant vesicles viewed with high temporal resolution. *Biophys. J.* 88: 1143–1155.

17. Tekle, E., H. Oubrahim, S. M. Dzekunov, J. F. Kolb, K. H. Schoenbach, and P. B. Chock. 2005. Selective field effects on intracellular vacuoles and vesicle membranes with nanosecond electric pulses. *Biophys. J.* 89:274–284.

18. Needham, D., and R. M. Hochmuth. 1989. Electro-mechanical permeabilization of lipid vesicles. Role of membrane tension and compressibility. *Biophys. J.* 55:1001–1009.

19. Kummrow, M., and W. Helfrich. 1991. Deformation of giant lipid vesicles by electric fields. *Phys. Rev. A.* 44:8356–8360.

20. Hyuga, H., K. Kinosita Jr., and N. Wakabayashi. 1993. Steady-state deformation of vesicle in alternating fields. *Bioelectrochem. Bioenerg.* 32:15–25.

21. Hyuga, H., K. Kinosita Jr., and N. Wakabayashi. 1991. Deformation of vesicles under the influence of strong electric fields. *Jpn. J. Appl. Phys.* 30:1141–1148.

22. Hyuga, H., K. Kinosita, Jr., and N. Wakabayashi. 1991. Deformation of vesicles under the influence of strong electric fields II. *Jpn. J. Appl. Phys.* 30:1333–1335.

23. Niggemann, G., M. Kummrow, and W. Helfrich. 1995. The bending rigidity of phosphatidylcholine bilayers: dependences on experimental method, sample cell sealing and temperature. *J. Phys. II France.* 5: 413–425.

24. Mitov, M., P. Méléard, M. Winterhalter, M. I. Angelova, and P. Bothorel. 1993. Electric-field-dependent thermal fluctuations of giant vesicles. *Phys. Rev. E.* 48:628–631.

25. Peterlin, P., S. Svetina, and B. Žekś. 2000. The frequency dependence of phospholipid vesicle shapes in an external electric field. Pflügers Arch. *Eur. J. Physiol.* 439:R139–R140.

26. Hyuga, H., K. Kinosita Jr., and N. Wakabayashi. 1991. Transient and steady-state deformations of a vesicle with an insulating membrane in response to step-function of alternating electric fields. *Jpn. J. Appl. Phys.* 30:2649–2656.

27. Dimova, R., S. Aranda, N. Bezlyepkina, V. Nikolov, K. A. Riske, and R. Lipowsky. 2006. A practical guide to giant vesicles. Probing the membrane nanoregime via optical microscopy. *J. Phys. Condens. Matter.* 18:S1151–S1176.

28. Iglesias, F. J., M. C. Lopes, C. Santamaria, and A. Dominguez. 1985. Orientation of *Schizosaccharomyces pombe* nonliving cells under alternating uniform and nonuniform electric fields. *Biophys. J.* 48: 712–726.

29. Neumann, E., S. Kakorin, and K. Toensing. 1998. Membrane electroporation and eletromechanical deformation of vesicles and cells. *Faraday Discuss.* 111:111–125.

30. Griese, T., S. Kakorin, and E. Neumann. 2002. Conductometric and electrooptic relaxation spectrometry of lipid vesicle electroporation at high fields. *Phys. Chem. Chem. Phys.* 4:1217–1227.

31. Kakorin, S., and E. Neumann. 2002. Electrooptical relaxation spectroscopy of membrane electroporation in lipids vesicles. *Colloids Surf. A.* 209:147–165.

32. Rodriguez, N., J. Heuvingha, F. Pincetb, and S. Cribier. 2005. Indirect evidence of submicroscopic pores in giant unilamelar vesicles. *Biochim. Biophys. Acta.* 1724:280–287.

33. Angelova, M. I., and D. S. Dimitrov. 1986. Liposome electroformation. *Faraday Discuss. Chem. Soc.* 81:303–311.

34. Dimova, R., U. Seifert, B. Pouligny, S. Förster, and H.-G. Döbereiner. 2002. Hyperviscous diblock copolymer vesicles. *Eur. Phys. J. B.* 7: 241–250.

35. Sinn, C., M. Antonietti, and R. Dimova. 2006. Binding of calcium to phosphatidylcholine-phosphatidylserine membranes. *Colloids Surf. A.* 282–283:410–419.

36. Miklavčič, D., D. Šemrov, H. Mekid, and L. M. Mir. 2000. A validated model of in vivo electric field distribution in tissues for electrochemotherapy and for DNA electrotransfer for gene therapy. *Biochim. Biophys. Acta.* 1523:73–83.

37. Gabriel, B., and J. Teissié. 1997. Direct observation in the millisecond time range of fluorescent molecule asymmetrical interaction with the electropermeabilized cell membrane. *Biophys. J.* 73:2630–2637.

38. Gabriel, B., and J. Teissié. 1999. Time courses of mammalian cell electropermeabilization observed by millisecond imaging of membrane property changes during the pulse. *Biophys. J.* 76:2158–2165.

39. Mutz, M., and H. Helfrich. 1990. Bending rigidities of some biological model membranes as obtained from Fourier analysis of contour sections. *J. Phys. France.* 51:991–1002.

40. Needham, D. 1995. Cohesion and permeability of lipid bilayer vesicles. *In* Permeability and Stability of Lipid Bilayers. E.A. Disalvo and S.A. Simon, editors. CRC Press, Boca Raton, FL. 49–76.

41. Abidor, I. G., V. B. Arakelyan, L. V. Chernomordik, Y. A. Chizmadzhev, V. F. Pastushenko, and M. R. Tarasevich. 1979. Electric breakdown of bilayer lipid membranes I. The main experimental facts and their qualitative discussion. *J. Electroanal. Chem.* 104:37–52.

42. Harbich, W., and W. Helfrich. 1979. Alignment and opening of giant lecithin vesicles by electric fields. *Z. Naturforsch.* 34a:1063–1065.

43. Kinosita, K. Jr., and T. Y. Tsong. 1979. Voltage-induced conductance in human erythrocyte membranes. *Biochim. Biophys. Acta.* 554: 479–497.

44. Korlach, J., C. Reichle, T. Müller, T. Schnelle, and W. W. Webb. 2005. Trapping, deformation, and rotation of giant unilamellar vesicles in octode dielectrophoretic field cages. *Biophys. J.* 89:554–562.

45. Sandre, O., C. Ménager, J. Prost, V. Cabuil, J.-C. Bacri, and A. Cebers. 2000. Shape transitions of giant liposomes induced by an anisotropic spontaneous curvature. *Phys. Rev. E.* 62:3865–3870.

46. Kinosita, K., Jr., I. Ashikawa, N. Saita, H. Yoshimura, H. Itoh, K. Nagayama, and A. Ikegami. 1988. Electroporation of cell membrane visualized under a pulsed-laser fluorescence microscope. *Biophys. J.* 53:1015–1019.

47. Cevc, G., editor. 1993. Phospholipids Handbook. Marcel Dekker, New York.

48. Simon, S. A., and T. J. McIntosh. 1986. Depth of water penetration into bilayers. *Methods Enzymol.* 127:511–521.